Lotus seedpod as a low-cost biomass for potential methylene blue adsorption

Qiulai He, Hongyu Wang, Jing Zhang, Zhuocheng Zou, Jun Zhou, Kai Yang and Lian Zheng

ABSTRACT

The adsorption of methylene blue (MB) by low cost biomass lotus seedpod (LSP) was optimized by a central composite design combined with response surface methodology in aqueous solution. Solution pH, initial dye concentration and adsorbent dosage were studied as independent variables at five levels each, respectively. Analysis of variance suggested the validity of the regression model. LSP was characterized by Fourier transform infrared spectra and energy dispersive spectroscopy. The kinetics revealed that the adsorption behavior followed the pseudo-second-order model. Langmuir and Freundlich isotherm models were used to evaluate the adsorption, and the experimental data were better fitted by the Langmuir isotherm than the Freundlich isotherm. The maximum monolayer adsorption capacity of the LSP was 157.98 mg g^{-1} at 30 °C for MB adsorption. In addition, 0.2 M HCl solution could be used for reusability of LSP via desorption tests. LSP was proven to be an available and effective biosorbent for MB removal from aqueous solution.

Key words | adsorption, isotherms, kinetics, lotus seedpod, methylene blue, response surface methodology

Qiulai He
Hongyu Wang (corresponding author)
Jing Zhang
Zhuocheng Zou
Jun Zhou
Kai Yang
School of Civil Engineering, Wuhan University,
Wuhan 430072,
China
E-mail: *hywang96@126.com*

Lian Zheng
Central and Southern China Municipal Engineering Design & Research Institute Co. Ltd,
Wuhan 430072,
China

INTRODUCTION

Dyes from industrial effluents such as textile, paper, plastics and leather are great concerns due to their high visibility, undesirability and recalcitrance (Roosta *et al.* 2014), which can cause severe damage to both humans and the environment (Han *et al.* 2011). Methylene blue (MB) (3,7-bis (dimethylamino)-phenothiazin-5-ium chloride) has been widely used for coloring paper, temporary hair colorant, dyeing cottons and so on (Iriarte-Velasco *et al.* 2015). MB can cause eye burns in both human and animals, which may be responsible for permanent injury to the eyes (Kavitha & Namasivayam 2007). Therefore, it is necessary to find low-cost and effective ways of removing MB from industrial wastewater to reduce environmental problems.

Adsorption has been testified to be an available approach for MB removal due to the high efficiency, capacity and large scale ability of generable adsorbents, though many other technologies such as flocculation, coagulation, precipitation, membrane filtration, electrochemical techniques, and ozonation have also been applied (Bestani *et al.* 2008). The design of novel procedures based on non-toxic, low-cost and easily available adsorbents is the best choice for MB removal. Numerous researches have been conducted to utilize low-cost adsorbents for removal of MB, including bamboo (Mui *et al.* 2010), coffee beans (Franca *et al.* 2009), fruit shell (Noorimotlagh *et al.* 2014), and vine shoots (Ruiz-Fernandez *et al.* 2010) and so on. Lotus seedpod (*Nelumbo nucifera*, (LSP)), as a waste biomass from an agricultural byproduct, is widespread in China, especially in Hubei Province (Han *et al.* 2011). LSP contains abundant floristic fiber, protein and some functional groups that may contribute to the adsorption process, like other plant materials (Han *et al.* 2007).

However, the adsorption efficiency depends on several independent variables such as solution pH, initial dye concentration, adsorbent dosage and so on (Cao *et al.* 2014). Response surface methodology (RSM) with analysis of variance (ANOVA) as a mathematical statistical technique has long been used to optimize all the process independent variables (Auta & Hameed 2011; Pandey & Negi 2015), which can evaluate the relative significance of the variables even in the presence of complex factor-factor interactions (Ghaedi *et al.* 2015). Hence, central composite design (CCD) under

doi: 10.2166/wst.2016.423

RSM using ANOVA can be applied to maximize the criterion of the response. A comparison between the results from the present models and the experimental values is also conducted during the process.

In the present study, the objective was to investigate the adsorption of MB by low-cost biomass LSP from aqueous solution and to optimize the independent parameters for maximal removal efficiency by RSM using ANOVA. The LSP before and after adsorption was characterized by Fourier transform infrared (FTIR) spectra and energy dispersive spectroscopy (EDS). The adsorption mechanism was also determined by calculating the kinetics. Different isotherm models, including Langmuir and Freundlich, were utilized to fit the adsorption process. Desorption experiments were also conducted to investigate the reusability of LSP. This study reports for the first time on the availability and feasibility of low-cost biomass LSP as an alternative adsorbent for MB removal.

MATERIALS AND METHODS

LSP preparation

LSP was collected from the East Lake, Wuhan, China. Prior to experiments, the LSP was thoroughly washed with running water for several hours to remove dust and then washed with distilled water. The clean LSP was then oven-dried at 105 °C overnight. Dried materials were cut into small pieces, and then ground into powder. Only fine particles passing through a 50 meshsieve (corresponding to 297 μm in diameter) were used for the present study.

Batch adsorption experiments

Batch experiments were conducted in a series of 50 mL flasks by shaking 0.04 g LSP with 40 mL of predetermined concentrations of MB solution in a mechanical shaker at 180 rpm, 30 °C for 4 h. The initial pH (around 7.0) was not controlled otherwise for the RSM optimization tests. The adsorption kinetics were determined by shaking 0.04 g LSP with 40 mL of 100 mg L^{-1} MB solution at a constant temperature of 30 °C. The residual MB concentration in the supernatant was determined at certain intervals. Adsorption isotherms were performed by agitating 40 mL of MB solution at concentrations from 10 to 500 mg L^{-1} at 30 °C. After adsorption, the LSP was separated from the MB solution and the supernatants were analyzed according to the method by (Sun *et al.* 2015). All experiments were conducted in triplicate, and the average values were used for statistical analysis.

The adsorption capacity q_e (mg g^{-1}) and removal efficiency (%) were determined by Equations (1) and (2), respectively:

$$q_e = \frac{(C_0 - C_e)V}{M} \tag{1}$$

$$\text{Removal}\,(\%) = \frac{C_0 - C_e}{C_0} \times 100 \tag{2}$$

where C_o and C_e are the initial and equilibrium MB concentrations, respectively (mg L^{-1}), V is the volume of MB solution (L), and M is the amount of LSP (g).

Desorption experiments

During the desorption process, 0.02 g of the MB-loaded LSP was separated, and was then reused and stirred with 40 mL of HCl solution at various concentrations (0, 0.2, 0.4, 0.6, 0.8 and 1.0 mol L^{-1}) for 4 h. The desorption efficiency was determined by analyzing the MB concentration in the supernatant solution after centrifugation.

Optimization of the experimental design

A CCD under RSM was used to investigate the three independent variables: the initial pH (X_1), MB concentration (X_2) and adsorbent dosage (X_3) on MB removal at five levels in aqueous solution (Table 1). The adsorption of MB onto LSP was explained by the following second-order polynomial model (Savasari *et al.* 2015):

$$Y = \beta_0 + \Sigma\beta_i X_i + \Sigma\beta_{ii} X_i^2 + \Sigma\beta_{ij} X_i X_j + \epsilon \tag{3}$$

where Y is the predicted response, the terms β_0, β_i, β_{ii}, β_{ij} and ε are the offset term, linear effect, squared effect,

Table 1 | Experimental variables and their coded levels for CCD

	Range and levels (coded)				
Factors	**−2**	**−1**	**0**	**1**	**2**
X_1: pH	1	3	5	7	10
X_2: MB concentration (mg·L^{-1})	10	50	100	200	500
X_3: Dosage (mg·L^{-1})	0.5	1	2	3	5

interaction effect and residual term, respectively. X_i and X_j are the coded variables.

Design expert version 8 (Stat-Ease, USA) was used to optimize the levels of the independent variables, evaluate the interactions of the process factors, and for regression and graphical analysis of data. The removal efficiency was set as the output response.

RESULTS AND DISCUSSION

Characteristics of LSP

Figure 1 shows the FTIR spectra for LSP before (a) and after (b) adsorption of MB. Both samples displayed a broad and strong band with peaks at 3,423 and 3,427 cm^{-1}, which was due to the stretch vibration of bonded –OH on the surface of the LSP (Pandey & Negi 2015). The asymmetric stretch vibration of $-CH_3$ could be seen at 2,924 cm^{-1}, while the symmetric stretch vibration of $-CH_2$ led to the adsorption peak at 2,854 cm^{-1} (Han *et al.* 2011). The strong peak at 1,622 cm^{-1} corresponded to C=O stretching vibrations typical of carboxylate moieties, while the small peaks at 1,525 and 1,446 cm^{-1} were attributed to the aromatic rings and symmetric bending of $-CH_3$, respectively (Cao *et al.* 2014). The asymmetric bending vibrations of $-CH_3$ and $-CH_2$ could be seen at peaks near 1,378–1,388 cm^{-1}. The additional peak at 1,062 cm^{-1} indicated the S=O stretching vibration (Noorimotlagh *et al.* 2014). Upon MB loading, the FTIR spectrum had no significant change apart from some intensity increases and vibrations and bonds shifts. The results of FTIR analysis revealed some potential active sites for adsorption such as carbonyl and hydroxyl groups (Kavitha & Namasivayam 2007).

Figure 2(a) and 2(b) present the EDS results of LSP before and after adsorption of MB, respectively. The presence of typical elements in biomass, including carbon, oxygen, phosphorus magnesium, potassium, calcium and iron, was commonly detected relatively abundantly in both samples. The presence of cationic elements like magnesium, potassium, calcium and iron might contribute to the adsorption of the MB anionic dye. In addition, the strong peak of sulfur confirmed the high adsorption capacity of LSP, for this element was abundant only in MB. Meanwhile, the higher abundance of carbon and oxygen within the sample after adsorption also confirmed the adsorption of MB onto LSP. The EDS spectrum also provided evidence of a large number of carbonyl and hydroxyl groups on the surface of the LSP before and after adsorption (Kavitha & Namasivayam 2007).

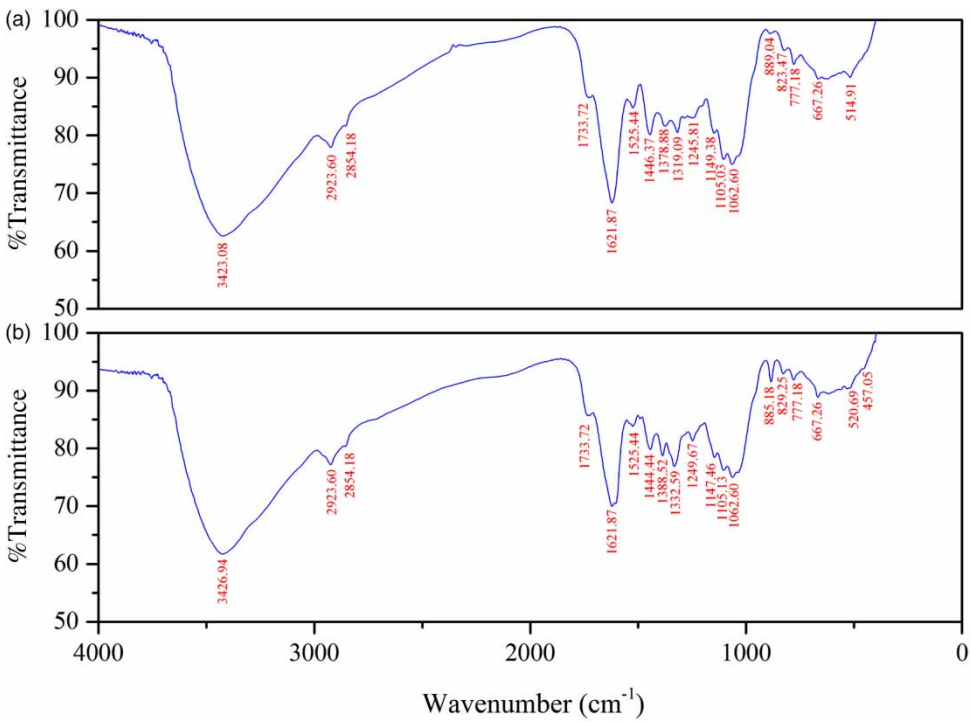

Figure 1 | FTIR of the LSP before and after adsorption of MB.

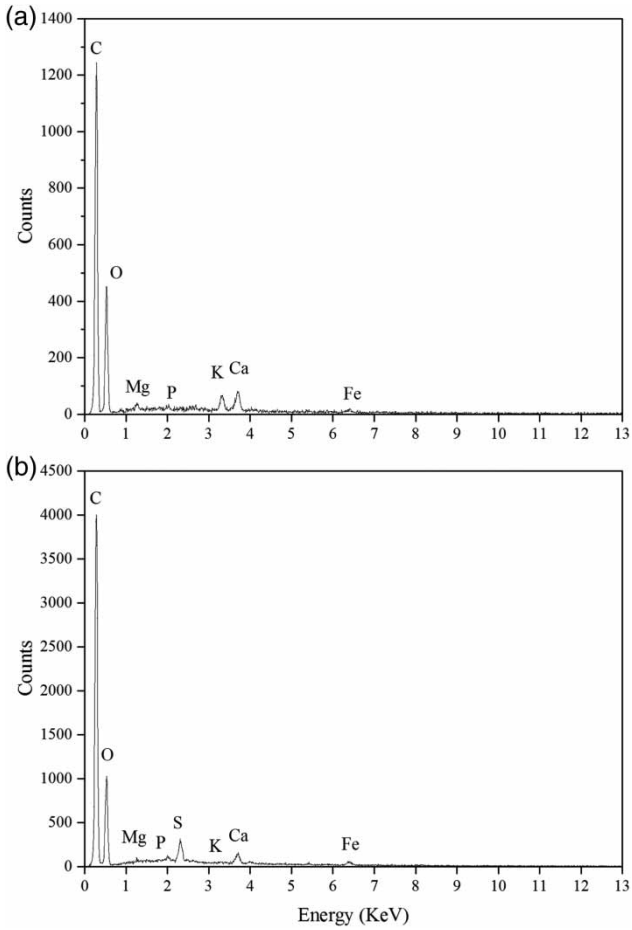

Figure 2 | EDS spectrum of LSP (a) before and (b) after adsorption of MB.

Optimization of the MB adsorption process

CCD model fitting and statistical analysis

A 20-run CCD experimental design (pH 1–10, initial concentration 10–500 mg L^{-1}, and dosage 0.5–5 mg L^{-1}) was carried out, and the results are shown in Table 2. The following second-order polynomial model equation describes the adsorption removal (%) of MB.

$$Y = 39.39 + 16.44X_1 - 0.13X_2 + 6.20X_3 + 8.08\times10^{-5}X_1X_2 - 0.30X_1X_3 + 0.04X_2X_3 - 1.08X_1^2 - 7.84\times10^{-5}X_2^2 - 1.28X_3^2 \quad (4)$$

Each actual value was compared with the predicted value from the above Equation (4), and the residual was calculated by subtraction (Table 2). It was apparent that the predicted values were highly consistent with the actual ones, while the residuals were dispersed around zero with no particular pattern within the range of experiments, indicating good validity of the regression model given above (Pandey & Negi 2015).

To further ensure the validity of the above RSM model for MB adsorption, ANOVA analysis was conducted. The results of the fitting model, in the form of ANOVA, are given in Table 3. The *model F-value* of 227.69 implied the model was significant, since there was only a 0.01% chance that a '*model F-value*' this large could occur due to noise. Values of '*prob* > *F*' less than 0.05 indicated model terms were significant. Therefore, all terms including X_1, X_2, X_3, X_1X_2, X_1X_3, and X_2X_3 were significant model in this study. The '*Lack of Fit F-value*' of 226.52 implied the *Lack of Fit* was significant, which revealed that some systematic variations were unaccounted for in the hypothesized model. The exact replicate values of the independent variables in the model that provided an estimate of pure error could be responsible (Pandey & Negi 2015). A good agreement between the predicated and actual results was obtained due to the high values of the determination

Table 2 | Experimental design in terms of coded variables and results of the CCD

	Coded variable			Response (%)		
Run	X1	X2	X3	Actual	Predicted	Residual
1	3	200	3	81.08	82.20	– 1.12
2	7	50	3	100.00	100.00	– 0.01
3	5	100	2	95.17	94.31	0.86
4	3	50	3	83.11	83.23	– 0.13
5	5	100	2	95.37	94.31	1.06
6	7	200	3	99.90	100.00	– 0.10
7	5	100	2	95.17	94.31	0.86
8	7	50	1	99.41	100.00	– 0.59
9	10	100	2	93.72	92.27	1.45
10	5	100	0.5	84.51	85.10	– 0.60
11	3	50	1	78.97	79.02	– 0.05
12	3	200	1	64.01	63.46	0.55
13	1	100	2	56.41	57.07	– 0.66
14	5	500	2	61.20	60.96	0.23
15	5	10	2	98.69	98.73	– 0.04
16	5	100	2	95.13	94.31	0.81
17	5	100	2	95.00	94.31	0.69
18	5	100	5	96.00	95.13	0.87
19	7	200	1	84.04	83.40	0.64
20	5	100	2	95.23	94.31	0.91

Table 3 | ANOVA of the response surface quadratic model for MB adsorption

Source	Sum of squares	Degrees of freedom	Mean square	F value	*P*-value *prob* > *F*
Model	3389.56	9	376.62	227.69	<0.0001
X_1	685.72	1	685.72	414.55	<0.0001
X_2	58.86	1	58.86	35.58	0.0001
X_3	21.44	1	21.44	12.96	0.0048
X_1X_2	0.00	1	0.00	0.00	0.9787
X_1X_3	2.83	1	2.83	1.71	0.2200
X_2X_3	94.00	1	94.00	56.83	<0.0001
X_1^2	759.84	1	759.84	459.36	<0.0001
X_2^2	31.94	1	31.94	19.31	0.0013
X_3^2	74.63	1	74.63	45.12	<0.0001
Residual	16.54	10	1.65		
Lack of Fit	16.47	5	3.29	226.52	<0.0001
Pure Error	0.073	5	0.015		
Cor Total	3406.10	19			

$R^2 = 0.995$, adj. $R^2 = 0.991$

coefficient ($R^2 = 0.995$) and the adjusted determination coefficient (adj. $R^2 = 0.991$).

Model interpretation and optimization of variables

Three-dimensional (3D) surface plots were generated to reveal the behavior of the experimental design system within two factors, holding the other factor at central level (Liu *et al.* 2010). The effects of the experimental variables on the responses are presented in the 3D plots in Figure 3.

Figure 3(a) and 3(b) reveal the influence of initial solution pH on the adsorption removal efficiency. It was obvious that the removal rate increased via a pH ranging from 3.0 to 7.0. Within the pH range from 1.0 to 10.0, the removal rate increased sharply from 50% at pH 1.0 to 95% at pH 7.5, and then decreased to 88% at pH 10.0. Solution pH was a vital factor due to its effects on both the LSP and the MB (Kavitha & Namasivayam 2007). An alkaline environment was more favorable for the adsorption process of MB onto LSP for the cationic dye reaction with OH^-, which would be suppressed by H^+ in acidic conditions (Han *et al.* 2011). The slight decrease in removal rate after pH 7.5 indicated that the electrostatic mechanism was not the only mechanism for MB adsorption by LSP. Han *et al.* (2007) reported that the chemical reaction between the adsorbent and dye molecules was another possible mechanism. Given the above results, the batch experiments were carried out without pH adjustment of the original MB (pH near 7.0).

The effect of the initial MB concentration on the removal rate is shown in Figure 3(a) and 3(c). Although the removal rate decreased with the increase in MB concentration, the equilibrium adsorption capacity increased, and the trend was more apparent at appropriate pH values. This could be explained by the larger mass transfer provided by higher MB concentration, which could overcome various resistances from the aqueous solution (Yi & Zhang 2008). However, the amount of adsorbed MB stayed unchanged at high MB concentrations, for the adsorption sites available were limited on the surface of the LSP, thus making the adsorption capacity decrease to some degree (Dural *et al.* 2011). Considering the removal efficiency and adsorption capacity, an initial concentration of around 100 mg L^{-1} was recommended for this study.

Figure 3(b) and 3(c) show the influence of LSP dosage on the removal efficiency of MB. It was obvious that the removal rates at different dosages were largely affected by the initial concentration. Within the initial concentration range from 10 to near 80 mg L^{-1}, the removal rate increased slowly; while an opposite trend was exhibited for removal efficiency at concentrations above 80 mg L^{-1}, with 2.75 g/L as a turning point for LSP dosage. This was due to the overlapping of the active sites in competition for excess adsorbents (Weng & Pan 2007). Therefore, a dosage of about 2.75 g L^{-1} was recommended for high concentrations (above 200 mg L^{-1}) of MB while at low concentrations (lower than 200 mg L^{-1}) 1 g L^{-1} of adsorbent was enough.

Adsorption kinetics and isotherms

Adsorption kinetics

Pseudo-first-order and pseudo-second-order models were used to evaluate the kinetic mechanism that controlled the adsorption process. The linear forms of pseudo-first-order (Kannan & Sundaram 2001) and pseudo-second-order (Ho & McKay 1998) equations were given as follows:

$$\frac{1}{q_t} = \frac{1}{q_1} + \frac{1}{q_1}\left(\frac{1}{t}\right) \tag{5}$$

$$\frac{t}{q_t} = \frac{1}{k_2 q_2^2} + \frac{1}{q_2}t \tag{6}$$

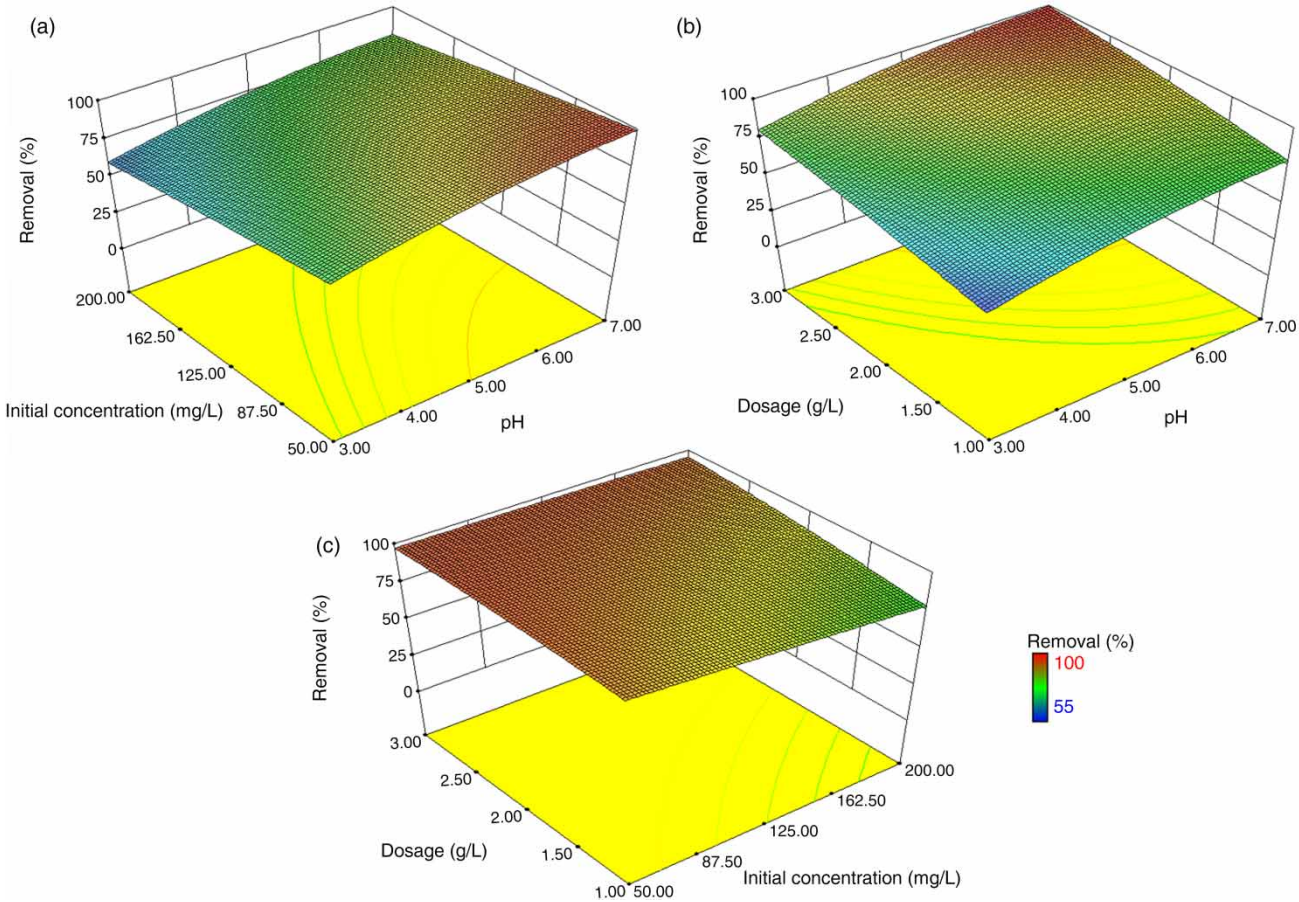

Figure 3 | Response surface plots for combined effect of (a) pH and initial concentration, (b) pH and dosage, and (c) initial concentration and dosage.

where q_1, q_2 and q_t are the amount of MB adsorbed at equilibrium and at time t, in mg·g^{-1}, k_1 (min^{-1}) and k_2 (g mg^{-1} min^{-1}) are the rate constants. The plots are presented in Figure 4, while the calculated kinetic models and related constants with linear regression coefficient (R^2) are shown in Table 4.

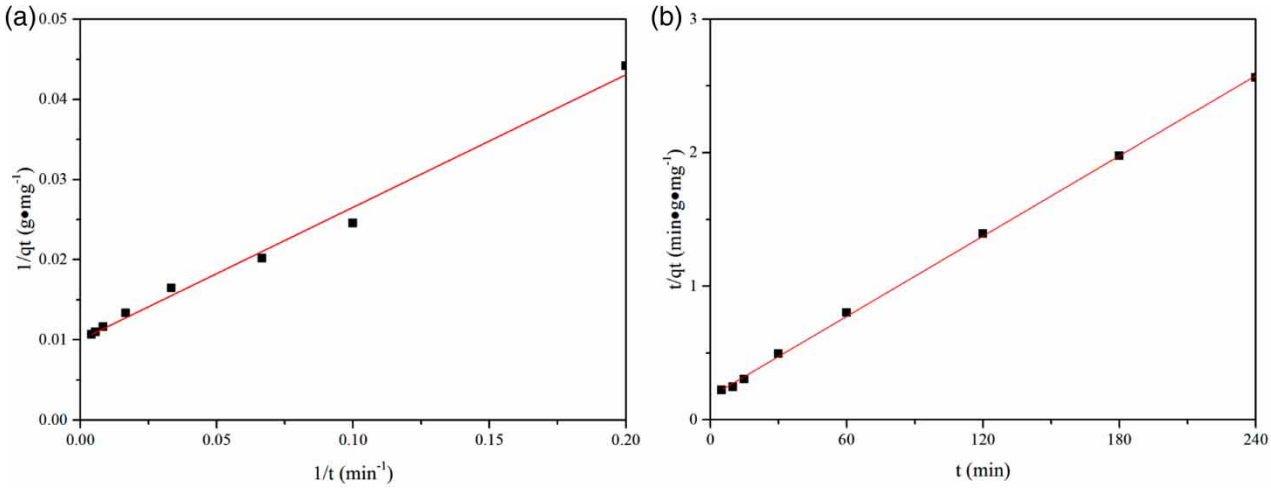

Figure 4 | Kinetic plots for adsorption of MB onto LSP at 30 °C: (a) pseudo-first-order and (b) pseudo-second-order model.

Table 4 | Kinetic parameters for adsorption process at 30 °C

Pseudo-first-order			Pseudo-second-order		
k_1 (min^{-1})	q_1 (mg g^{-1})	R^2	$k_2 \times 10^4$ (g mg^{-1} min^{-1})	q_2 (mg g^{-1})	R^2
16.5165	99.9001	0.9906	5.8132	99.8004	0.9994

The results showed that the experimental values were better fitted by the pseudo-second-order than the pseudo-first-order model due to the higher R^2, though both models could well describe the adsorption process (0.9994 and 0.9906 for the pseudo-first-order and pseudo-second-order model, respectively). In addition, the theoretical q_2 value (99.8004 mg g^{-1}) agreed well with the experimental values at various initial concentrations. The kinetics indicated that chemical adsorption involving valency forces through the exchange or sharing of electrons between MB molecules and the LSP was the rate-limiting step of the adsorption mechanism (Hameed *et al.* 2007; Wang *et al.* 2015).

Adsorption isotherms

In this study, the Langmuir and Freundlich isotherms were employed to characterize the adsorption behavior. Both isotherms are stated below.

Langmuir isotherm:

$$\frac{C_e}{q_e} = \frac{1}{q_{\max} K_L} + \frac{C_e}{q_{\max}} \tag{7}$$

Freundlich isotherm:

$$\log q_e = \log K_F + \frac{1}{n} \log C_e \tag{8}$$

where q_e is the equilibrium MB concentration onto the LSP (mg g^{-1}), C_e is the equilibrium MB concentration in the solution phase (mg L^{-1}), q_{max} is the monolayer adsorption capacity of the LSP (mg g^{-1}), K_L (L mg^{-1}), K_F (L mg^{-1}) and n is the adsorption constant for the Langmuir and Freundlich isotherms, respectively. The plots of C_e/q_e versus C_e, log q_e versus log C_e are shown in Figure 5, and the isotherm parameters are given in Table 5.

The results indicated that the Langmuir model ($R^2 = 0.9995$) fitted the adsorption better than the Freundlich model ($R^2 = 0.9009$). Furthermore, the maximum adsorption capacity of MB by the LSP was 157.98 mg g^{-1} in the present conditions. Compared with the previous researches (Feng *et al.* 2012; Sun *et al.* 2013; Zhang *et al.* 2013; Sarat Chandra *et al.* 2015), the maximum monolayer adsorption of MB was at a relatively high level. Moreover, the K_L value of 0.67 L mg^{-1} also suggested that the LSP was an ideal adsorbent for MB removal (Han *et al.* 2011).

Desorption experiment

The adsorption reversibility of the MB loaded LSP was investigated using various concentrations of HCl solutions and the results are shown in Figure 6. It can be seen from Figure 6 that the maximum desorption capacity of 28.5 mg g^{-1} was obtained at 0.2 mol L^{-1} HCl. It stayed

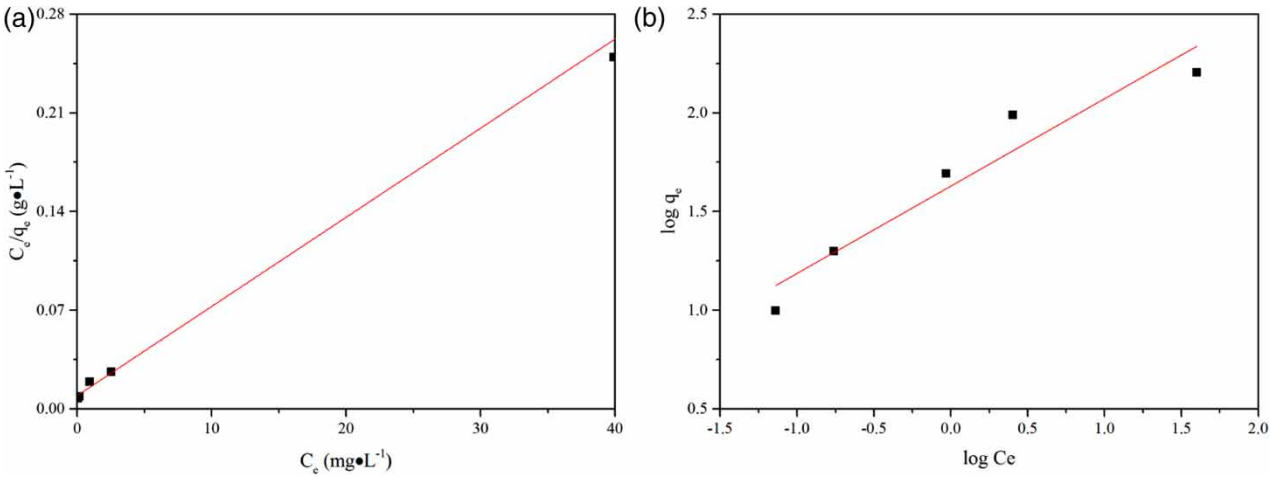

Figure 5 | Isotherm plots for adsorption of MB onto LSP: (a) Langmuir and (b) Freundlich isotherm.

Table 5 | Isotherm parameters for the adsorption of MB onto LSP at 30 °C

Langmuir			Freundlich		
q_{max} (mg·g^{-1})	K_L (L·mg^{-1})	R^2	K_F (L·mg^{-1})	n	R^2
157.9779	0.6734	0.9995	42.5177	2.2592	0.9009

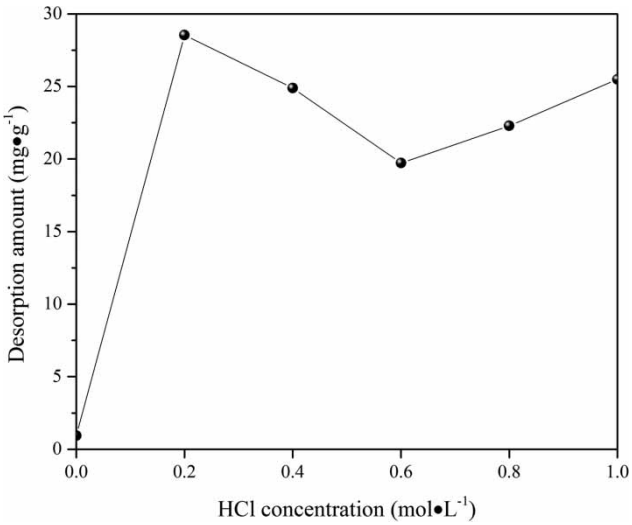

Figure 6 | Desorption performance at different concentrations of HCl solutions.

unaffected at about 23 mg g^{-1} at a desorption solution concentration above 0.4 mol L^{-1} HCl. The mechanism of desorption was probably the ion-exchange of MB with the H^+ on the surface of the LSP (Yi & Zhang 2008; Chen *et al.* 2015). Hence 0.2 mol L^{-1} HCl solution was best for desorption and reusability of LSP for MB adsorption.

CONCLUSIONS

The adsorption of MB onto low-cost biomass, LSP, from aqueous solution was investigated using RSM with initial pH, MB concentration and adsorbent dosage as independent variables. Good validity of the regression model was confirmed by analysis. The adsorption process was found to be consistent with the pseudo-second-order model. Both Langmuir and Freundlich isotherms were employed to evaluate the adsorption behavior with the maximum monolayer adsorption capacity of 157.98 mg g^{-1}. Desorption performance suggested that 0.2 mol L^{-1} HCl solution could be used for desorption and reusability of LSP. The results of FTIR and EDS analysis confirmed the availability of LSP as an effective adsorbent for MB adsorption.

ACKNOWLEDGEMENTS

This work was financially supported by the CRSRI Open Research Program (SN: CKWV2016399/KY), the Open Project of State Key Laboratory of Urban Water Resource and Environment, Harbin Institute of Technology (QA201614), and the National Natural Science Foundation of China (NSFC) (No. 51378400).

REFERENCES

Auta, M. & Hameed, B. H. 2011 Optimized waste tea activated carbon for adsorption of methylene blue and acid blue 29 dyes using response surface methodology. *Chemical Engineering Journal* **175**, 233–243.

Bestani, B., Benderdouche, N., Benstaali, B., Belhakem, M. & Addou, A. 2008 Methylene blue and iodine adsorption onto an activated desert plant. *Bioresource Technology* **99** (17), 8441–8444.

Cao, J. L., Wu, Y. H., Jin, Y. P., Yilihan, P. & Huang, W. F. 2014 Response surface methodology approach for optimization of the removal of chromium(VI) by NH_2-MCM-41. *Journal of the Taiwan Institute of Chemical Engineers* **45** (3), 860–868.

Chen, D., Yang, K., Wang, H. Y., Zhou, J. & Zhang, H. N. 2015 Cr (VI) removal by combined redox reactions and adsorption using pectin-stabilized nanoscale zero-valent iron for simulated chromium contaminated water. *Rsc Advances* **5** (80), 65068–65073.

Dural, M. U., Cavas, L., Papageorgiou, S. K. & Katsaros, F. K. 2011 Methylene blue adsorption on activated carbon prepared from *Posidonia oceanica* (L.) dead leaves: kinetics and equilibrium studies. *Chemical Engineering Journal* **168** (1), 77–85.

Feng, Y., Zhou, H., Liu, G., Qiao, J., Wang, J., Lu, H., Yang, L. & Wu, Y. 2012 Methylene blue adsorption onto swede rape straw (*Brassica napus* L.) modified by tartaric acid: equilibrium, kinetic and adsorption mechanisms. *Bioresource Technology* **125**, 138–144.

Franca, A. S., Oliveira, L. S. & Ferreira, M. E. 2009 Kinetics and equilibrium studies of methylene blue adsorption by spent coffee grounds. *Desalination* **249** (1), 267–272.

Ghaedi, A. M., Ghaedi, M., Vafaei, A., Iravani, N., Keshavarz, M., Rad, M., Tyagi, I., Agarwal, S. & Gupta, V. K. 2015 Adsorption of copper (II) using modified activated carbon prepared from Pomegranate wood: optimization by bee algorithm and response surface methodology. *Journal of Molecular Liquids* **206**, 195–206.

Hameed, B. H., Din, A. T. & Ahmad, A. L. 2007 Adsorption of methylene blue onto bamboo-based activated carbon: kinetics and equilibrium studies. *Journal of Hazardous Materials* **141** (3), 819–825.

Han, R., Zou, W., Yu, W., Cheng, S., Wang, Y. & Shi, J. 2007 Biosorption of methylene blue from aqueous solution by fallen phoenix tree's leaves. *Journal of Hazardous Materials* **141** (1), 156–162.

Han, X. L., Wang, W. & Ma, X. J. 2011 Adsorption characteristics of methylene blue onto low cost biomass material lotus leaf. *Chemical Engineering Journal* **171** (1), 1–8.

Ho, Y. S. & McKay, G. 1998 Kinetic models for the sorption of dye from aqueous solution by wood. *Process Safety and Environmental Protection* **76** (B2), 183–191.

Iriarte-Velasco, U., Sierra, I., Cepeda, E. A., Bravo, R. & Ayastuy, J. L. 2015 Methylene blue adsorption by chemically activated waste pork bones. *Coloration Technology* **131** (4), 322–332.

Kannan, N. & Sundaram, M. M. 2001 Kinetics and mechanism of removal of methylene blue by adsorption on various carbons – a comparative study. *Dyes and Pigments* **51** (1), 25–40.

Kavitha, D. & Namasivayam, C. 2007 Experimental and kinetic studies on methylene blue adsorption by coir pith carbon. *Bioresource Technology* **98** (1), 14–21.

Liu, Y., Zheng, Y. A. & Wang, A. Q. 2010 Response surface methodology for optimizing adsorption process parameters for methylene blue removal by a hydrogel composite. *Adsorption Science & Technology* **28** (10), 913–922.

Mui, E. L., Cheung, W. H., Valix, M. & McKay, G. 2010 Dye adsorption onto char from bamboo. *Journal of Hazardous Materials* **177** (1–3), 1001–1005.

Noorimotlagh, Z., Soltani, R. D. C., Khataee, A. R., Shahriyar, S. & Nourmoradi, H. 2014 Adsorption of a textile dye in aqueous phase using mesoporous activated carbon prepared from Iranian milk vetch. *Journal of the Taiwan Institute of Chemical Engineers* **45** (4), 1783–1791.

Pandey, A. K. & Negi, S. 2015 Impact of surfactant assisted acid and alkali pretreatment on lignocellulosic structure of pine foliage and optimization of its saccharification parameters using response surface methodology. *Bioresource Technology* **192**, 115–125.

Roosta, M., Ghaedi, M., Daneshfar, A., Sahraei, R. & Asghari, A. 2014 Optimization of the ultrasonic assisted removal of methylene blue by gold nanoparticles loaded on activated carbon using experimental design methodology. *Ultrasonics Sonochemistry* **21** (1), 242–252.

Ruiz-Fernandez, M., Alexandre-Franco, M., Fernandez-Gonzalez, C. & Gomez-Serrano, V. 2010 Adsorption isotherms of methylene blue in aqueous solution onto activated carbons developed from vine shoots (Vitis Vinifera) by physical and chemical methods. *Adsorption Science & Technology* **28** (8–9), 751–759.

Sarat Chandra, T., Mudliar, S. N., Vidyashankar, S., Mukherji, S., Sarada, R., Krishnamurthi, K. & Chauhan, V. S. 2015 Defatted algal biomass as a non-conventional low-cost adsorbent: surface characterization and methylene blue adsorption characteristics. *Bioresource Technology* **184**, 395–404.

Savasari, M., Emadi, M., Bahmanyar, M. A. & Biparva, P. 2015 Optimization of Cd(II) removal from aqueous solution by ascorbic acid-stabilized zero valent iron nanoparticles using response surface methodology. *Journal of Industrial and Engineering Chemistry* **21**, 1403–1409.

Sun, L., Wan, S. & Luo, W. 2013 Biochars prepared from anaerobic digestion residue, palm bark, and eucalyptus for adsorption of cationic methylene blue dye: characterization, equilibrium, and kinetic studies. *Bioresource Technology* **140**, 406–413.

Sun, L., Chen, D., Wan, S. & Yu, Z. 2015 Performance, kinetics, and equilibrium of methylene blue adsorption on biochar derived from eucalyptus saw dust modified with citric, tartaric, and acetic acids. *Bioresource Technology* **198**, 300–308.

Wang, H., Gao, B., Wang, S., Fang, J., Xue, Y. & Yang, K. 2015 Removal of Pb(II), Cu(II), and Cd(II) from aqueous solutions by biochar derived from $KMnO_4$ treated hickory wood. *Bioresource Technology* **197**, 356–362.

Weng, C. H. & Pan, Y. F. 2007 Adsorption of a cationic dye (methylene blue) onto spent activated clay. *Journal of Hazardous Materials* **144** (1–2), 355–362.

Yi, J. Z. & Zhang, L. M. 2008 Removal of methylene blue dye from aqueous solution by adsorption onto sodium humate/polyacrylamide/clay hybrid hydrogels. *Bioresource Technology* **99** (7), 2182–2186.

Zhang, J., Ping, Q. W., Niu, M. H., Shi, H. Q. & Li, N. 2013 Kinetics and equilibrium studies from the methylene blue adsorption on diatomite treated with sodium hydroxide. *Applied Clay Science* **83–84**, 12–16.

First received 29 March 2016; accepted in revised form 23 August 2016. Available online 19 September 2016